ELSEVIER

S0032-3861(96)00477-6

Polymer Vol. 38 No. 1, pp. 177–182, 1997

0032-3861/97/$17.00 + 0.00

Microstructure study of acrylic polymer–silica nanocomposite surface by scanning force microscopy

Makoto Motomatsu*
Joint Research Center for Atom Technology, Angstrom Technology Partnership, 1-1-4 Higashi, Tsukuba, Ibaraki 305, Japan

and Tatsuhiro Takahashi
Advanced Materials Application Laboratory, DuPont Kabushiki Kaisha, 2-2-1 Hayabuchi, Tsuzuki-ku, Yokohama, Kanagawa 224, Japan

and Heng-Yong Nie, Wataru Mizutani and Hiroshi Tokumoto
Joint Research Center for Atom Technology, National Institute for Advanced Interdisciplinary Research, 1-1-4 Higashi, Tsukuba, Ibaraki 305, Japan
(Received 8 January 1996; revised 3 April 1996)

Scanning force microscopy (SFM) was successfully used to study the microstructures of acrylic polymer–silica nanocomposite surfaces processed by the sol–gel method. We observed excellent flatness of the dip-coated nanocomposite surfaces (root mean square roughness = 0.345 nm; mean roughness = 0.270 nm), probably due to the levelling effect of the dipping solution. SFM revealed that acrylic polymer and silica were hybridized on surfaces, with domain sizes from several to 30 nm, where friction forces between silica and acrylic polymer against the Si_3N_4 SFM tip were 35 and 1.6 nN respectively, for a 0.1 nN load. Copyright © 1996 Elsevier Science Ltd.

(Keywords: scanning force microscopy; nanocomposite; sol–gel method)

INTRODUCTION

Organic–inorganic hybrid nanocomposites have enormous potential applications since we can design such materials so that they compensate each other for unfavourable properties of the other component. For example, the properties of a gas barrier or weather-proofing of organic materials will be improved and flexibility or impact strength will be added to inorganic materials. There are numerous combinations in selecting preferential properties of the materials. In addition, it has been shown that inorganic materials with controlled pores can be obtained by removing organic polymer components by using selective solvents or baking at 600°C or higher[1]. Among these hybrid materials, those prepared from organic polymers and silicon alkoxides {mainly tetraethoxysilane $[Si(OC_2H_5)_4]$} by sol–gel processing have been widely studied, because the reaction speed is easily controllable. The sol–gel processed hybrid materials have interpenetrating polymer networks in the glassy network formed by polymerization[2–4]. Since the reaction takes place at room temperature, the process causes no thermal damage to organic molecular structures.

Structural studies of such hybrid nanocomposites have been mainly discussed for bulk materials and have shown that they are hybridized on a nanometre to micrometre scale, which is controllable by choosing solvents, mixing ratio, processing temperature, etc. However, few reports have focused on surface structures, probably because there have not been any suitable methods to observe nanometre-scale structures on surfaces in a real space, although it is of great interest to compare surface and inside structures. Scanning force microscopy (SFM)[5–7], followed by the invention of scanning tunnelling microscopy[8], enables us to observe surface structural details of non-conductive materials, together with the distribution of local mechanical properties that are specific to individual components[9–11]. The advantages of the SFM investigation are high spatial resolution and availability of topmost surface information, and surface preparation is not necessary. It has the high potential of becoming a novel characterization tool in replacement of existing methods where the beam size limits the spatial resolution and the beam causes damage to samples.

In the present paper we describe the observation of microstructural details and characterization of the topmost surface composition of acrylic polymer–silica nanocomposite on a nanometre scale by SFM.

EXPERIMENTAL

An acrylic polymer with a molecular weight of *ca* 11 000 (HEMA/BA/St/MMA/BMA = 37.3/36.3/20.0/4.4/2.0,

* To whom correspondence should be addressed

Table 1 Starting solution formula of acrylic polymer–silica nanocomposite

Ingredients	Weight (g)
Acrylic polymer	13
2-Propanol	10
2-Butoxyethanol	20
TEOS	30
6 N HCl	14

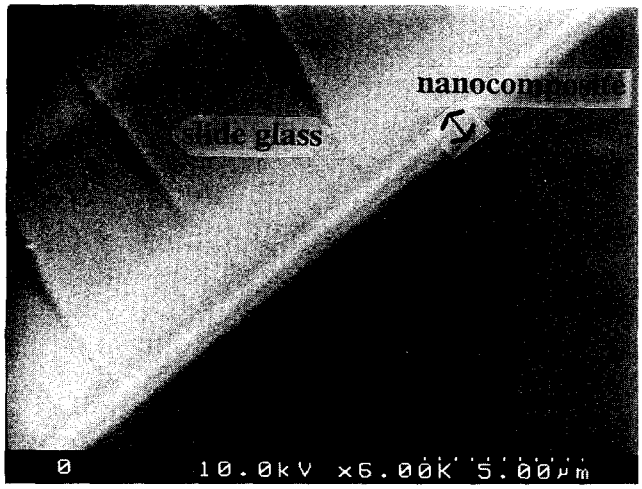

Figure 1 SEM micrograph of the cross-section of the acrylic polymer–silica nanocomposite film on the slide glass

where HEMA is 2-hydroxyethyl methacrylate, BA is butyl acrylate, St is styrene, MMA is methyl methacrylate, and BMA is isobutyl methacrylate) and tetraethoxysilane [TEOS: $Si(OC_2H_5)_4$, >99.9%] were used to prepare an organic–inorganic nanocomposite film by the sol–gel method. HEMA plays an important role in forming molecular-scale compatibility with the matrix network of the silica by the strong hydrogen bond between hydroxide groups of HEMA and silanol groups. The acrylic polymer and TEOS were dissolved in a mixed solution of 2-propanol (>99.9%) and 2-butoxyethanol (>99%) at room temperature and then hydrolysed and polycondensed by lastly adding HCl as catalyst to the stirred solution. This acrylic polymer and the above solution preparation were chosen to show no clouding of the nanocomposite and no sedimentation of the solution[12]. The formula of the solution is summarized in *Table 1*. The temperature of the solution increased because of the exothermic reaction. After the solution was cooled down to room temperature, the nanocomposite films were coated on to pre-cleaned slide glass substrates (S7213, Matsunami Glass Industry; contact angle against water ~ 0°) by a dip coating method at an upward drawing speed of 0.5 mm s^{-1}. The coated nanocomposite films were dried under vacuum (0.5 torr) at 120°C for 1 h. Some of them were heated at a heating ratio of 100°C h^{-1} and kept at 600°C for 2 h to eliminate the acrylic polymer (thermal decomposition) leading to porous silica formation. Films of pure acrylic polymer and pure silica were also prepared in the same manner to make a comparison with the nanocomposite film.

Contact angles against water were measured at room temperature by the free-standing drop method (~1.8 μl

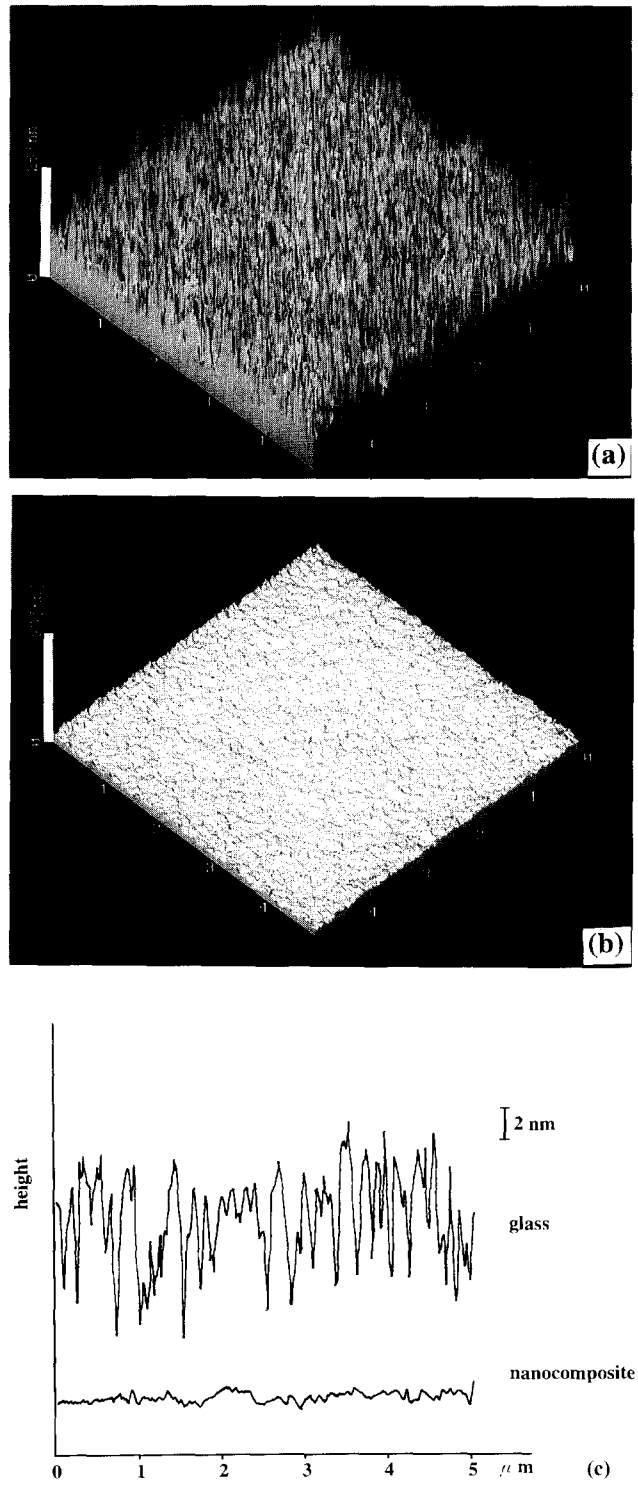

Figure 2 AFM topographic images of (a) the slide glass substrate, (b) the dip-coated acrylic polymer–silica nanocomposite film on a scan area of 5 μm × 5 μm, and (c) their typical one-dimensional topographies. The z axis is enhanced compared to the x or y axis, and the z scale in (a) and (b) is 25 nm. The RMS and R_a values are 3.19 and 2.60 nm in (a) and 0.345 and 0.270 nm in (b)

Table 2 Contact angles of nanocomposite, acrylic polymer and silica against water

Surface	Contact angle (degree)
Nanocomposite	72
Acrylic polymer	86
Silica	36

per drop) to estimate the macroscopic dispersion of the composite on surfaces.

SFM measurements were performed using an AFM instrument (SPA-300, Seiko Instruments Inc.) in the contact mode at 0.1 nN (calculated using the deflection of the cantilever) in air. A V-shaped micro-fabricated Si_3N_4 cantilever (Olympus Optics Inc.), with a spring constant of 0.1 N m^{-1} and pyramidal tip of *ca* 20 nm at the radius of the apex, was used. The local friction was measured using a four-segment photodiode system[13] (monitored by detecting the torsion of the cantilever) and its absolute value was estimated from the dimensions and the material of the cantilever and the sensitivity of the detection system, using the formula proposed by Meyer and Amer[14].

RESULTS AND DISCUSSION

The nanocomposite film obtained was transparent, indicating that the acrylic polymer and silica were hybridized on a smaller size than the visible wavelength. *Figure 1* shows a scanning electron microscope (SEM) micrograph of the cross-section of the nanocomposite film on the slide glass. The thickness was measured to be *ca* 800 nm by a stylus and SEM. *Figures 2a* and *b* show AFM topographic images of the slide glass substrate

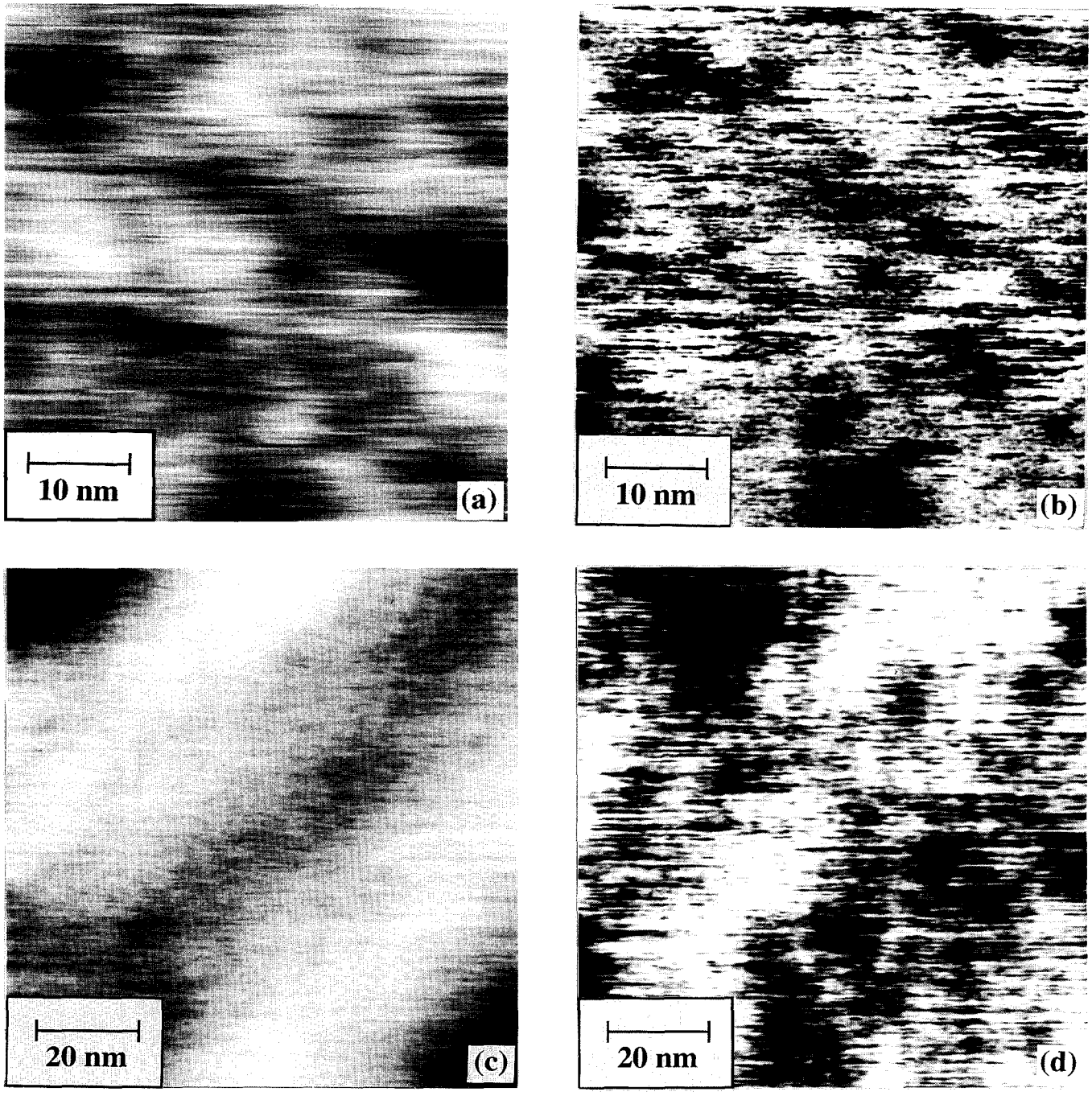

Figure 3 (a) AFM topographic image and (b) friction force image obtained simultaneously on a scan area of 50 nm × 50 nm, and (c) AFM topographic image and (d) friction force image obtained simultaneously on a scan area of 100 nm × 100 nm of the acrylic polymer–silica nanocomposite films. In (b) and (d), the bright region corresponds to higher friction (silica) and the dark region to lower friction (acrylic polymer)

Table 3 Estimated contact radii of acrylic polymer and silica using the bulk Young's modulus E_s and Poisson's ratio (ν_s) (AFM tip apex is estimated as a rigid sphere)

Material	E_s (GPa)	ν_s	Contact radius (nm)
Acrylic polymer	1–3	0.33	2.56–6.29
Silica	60	0.23	0.14

surface (without coating) and the coated nanocomposite surface, respectively, and *Figure 2c* shows typical one-dimensional topographies. The measured root mean square (RMS) and mean (R_a) roughness values for $5\,\mu m \times 5\,\mu m$ area were 3.19 and 2.60 nm for the slide glass substrate used here and 0.345 and 0.270 nm for the nanocomposite. This excellent flatness of the nanocomposite surface is probably due to the levelling characteristic of the dipping solution with the viscoelastic property, since surface tension is generally conceded to be the dominant force causing a liquid solution to level out[15].

Table 2 summarizes the contact angle results against water to compare the nanocomposite surface with those of the silica and the acrylic polymer. The data for the nanocomposite are between those for the acrylic polymer and the silica, indicating that both components exist on the surface, although contact angle data do not provide any information on surface structures. Because our nanocomposite surface is very flat, Cassie's law[16] on the smooth surface can be applied to estimate a surface area coverage macroscopically:

$$\cos\Phi_n = A_a \cos\Phi_a + A_s \cos\Phi_s \qquad (1)$$

Here, Φ_n is a measured contact angle on the nanocomposite, Φ_a that on pure acrylic polymer, and Φ_s that on pure silica; A_a is the surface area coverage ratio of acrylic polymer, and A_s that of silica. By applying the contact angle results in *Table 2* to equation (1), the surface area fraction of acrylic polymer on the nanocomposite surface was estimated to be 67.6% and that of silica to be 32.4%.

Typical SFM data on the nanocomposite surface are presented in *Figures 3a–d*. *Figure 3a* shows an AFM topographic image, and *Figure 3b* is the friction force image obtained at the same time. *Figures 3c* and *d* are another set of AFM topographic and friction force images taken simultaneously at a different position. Two types of domain consisting of lower and higher friction force regions are observed with a size of about 10 nm in *Figure 3b* and such domains are distributed in sizes from several to 30 nm at different positions, as shown in *Figure 3d*. The bright region corresponds to higher friction and the dark region to lower friction. Compared to these sets of images, the domain structures in friction force are not entirely commensurate with those of the topographic morphologies. Since the friction force is higher on the pure silica surface than on the pure acrylic polymer, it is concluded that the higher friction region corresponds to silica and the lower friction region to acrylic polymer. The pure silica surface showed 35 nN friction force while the pure acrylic polymer surface 1.6 nN friction force under the condition of a loading force of 0.1 nN and a velocity of $400\,nm\,s^{-1}$. The friction force is mainly influenced by the increase of contact area (softness of the material) and interaction between the sample and the probe material. For the estimation of contact area, the

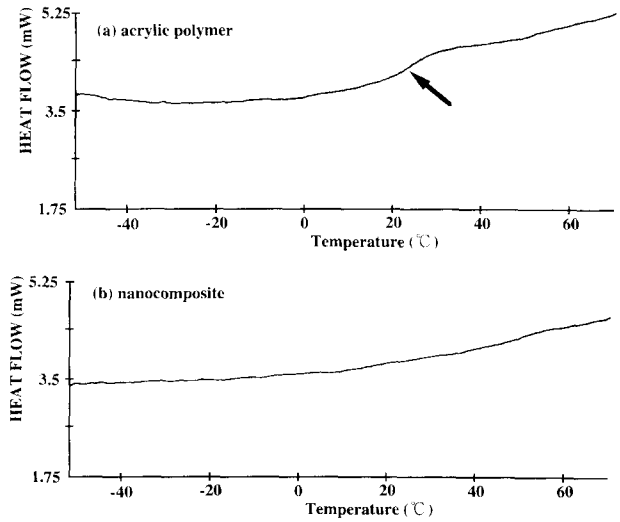

Figure 4 D.s.c. scans of (a) the pure acrylic polymer and (b) the nanocomposite. The glass transition of the acrylic polymer is 23°C as marked with an arrow. The heating rate was $10°C\,min^{-1}$

contact radii for both materials can be calculated using Sneddon's equation[17,18]:

$$F = \frac{E_s}{2(1-\nu_s^2)}\left[(\eta^2 + R^2)\ln\left(\frac{R+\eta}{R-\eta}\right) - \eta R\right] \qquad (2)$$

Here, E_s is Young's modulus, ν_s the Poisson ratio of the substrate material, η the contact radius, F the load, and R the radius of the AFM tip apex. *Table 3* summarizes the calculated contact radii and the used bulk data*[,19]. In this calculation, we employed a larger value for the loading force F of 90 nN because, as Burnham and Colton suggested[20], the extra force of the water meniscus is virtually dominant in air measurement. The estimated contact radii of the acrylic polymer and silica were 2.6–6.3 and 0.14 nm, respectively. Although the estimated contact radius of the acrylic polymer is much larger than that of silica, the friction force of the acrylic polymer by SFM is much smaller. We attribute this to the strong interaction between the SFM tip material of Si_3N_4 and SiO_2 surface. Thus, we conclude that the higher friction force area in *Figures 3b* and *d* corresponds to silica, and that the acrylic polymer and silica are hybridized on the surfaces in sizes of several to 30 nm. However, the fairly large contact area of the acrylic polymer (*Table 3*) cannot be negligible compared with the domain size, and the friction force of the acrylic polymer region on the nanocomposite films would be influenced by the surrounding silica during the scanning. Therefore, we cannot estimate the accurate surface fraction by SFM.

Here, we compare the result obtained by SFM with that of differential scanning calorimetry (d.s.c.) measurement[12], which provides the general information on compatibility with estimated phase-separated domain size of the structure inside. *Figure 4* shows d.s.c. scans on the pure acrylic polymer (a) and the nanocomposite (b). D.s.c. revealed a single glass transition temperature (T_g)

* We used typical values of E_s and ν_s of polymers as presented in *Table 3*. Poisson's ratio varies only slightly ($0 \leq \nu_s \leq 1$) and the contact area is appropriate for determining the local Young's modulus, since the quantity $E_s/(1-\nu_s^2)$ is dominated by E_s

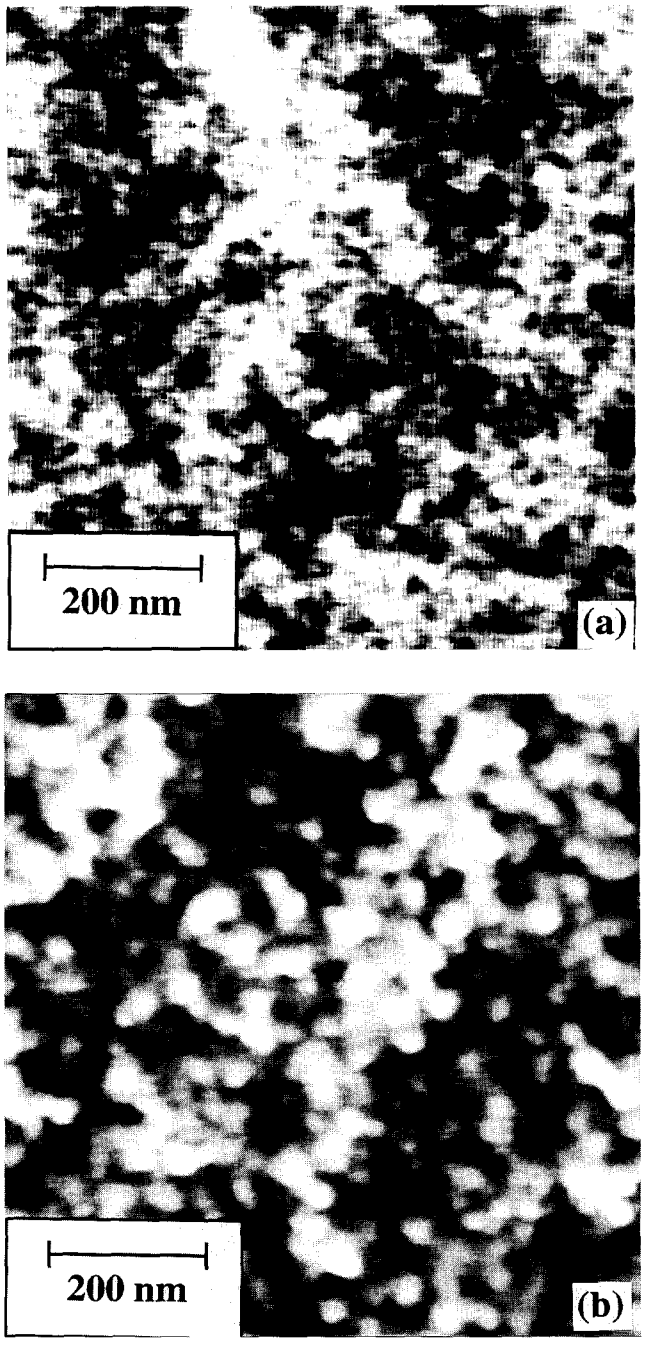

Figure 5 AFM topographic images of the acrylic polymer–silica nanocomposite film on a scan area of 800 nm × 800 nm (a) before and (b) after baking at 600°C for 2 h. The grey scale for the height in (a) is 1.87 nm and that in (b) is 2.47 nm

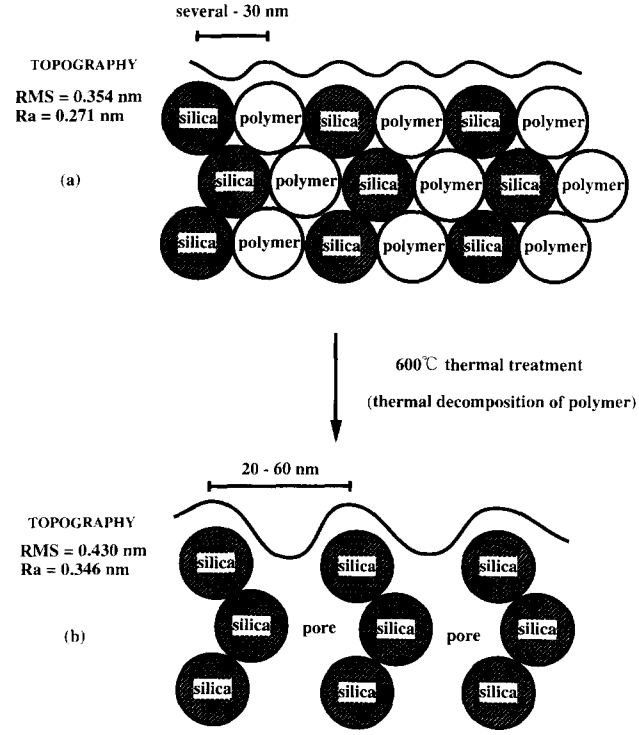

Figure 6 Schematic drawing of cross-sectional views of the surface structure of the acrylic polymer–silica nanocomposite film with the RMS and R_a roughness values (a) before and (b) after the thermal treatment at 600°C for 2 h

of 23°C for the pure acrylic polymer, while the nanocomposite sample did not show a sharp T_g point for the acrylic polymer. This indicates the homogeneous hybrid inside the nanocomposite[21] estimated by the disappearance of the T_g[22] point. The result leads us to conclude that the acrylic polymer and silica are hybridized with a size distribution of 2–15 nm in diameter inside the bulk due to the resolution limit of d.s.c. for the detection of the phase separation[23,24]. This value roughly agrees with the domain size on the surfaces obtained by SFM, and also with that on the poly(*N*-vinylpyrrolidone)–silica hybrid surfaces obtained by Saegusa[25].

Figures 5a and *b* show the AFM topographic images of the nanocomposite film before and after heat treatment at 600°C for 2 h, respectively. At 600°C, the acrylic polymer entirely decomposes and leaves porous silica behind. The contact angle of this heat-treated surface against water was 36°, which is the same as that of the pure silica surface (*Table 2*). Thus, the surface composition in *Figure 5b* should be silica alone. The RMS and R_a roughness values for 800 nm × 800 nm area in *Figures 5a* and *b* were measured to be 0.354 and 0.271 nm, and 0.430 and 0.346 nm, respectively, indicating the slight increase in the surface roughness by the heat treatment. In addition, in *Figure 5b*, the silica appears as particles, and the size is distributed from 20 to 60 nm. The change in the topography and morphology of the nanocomposite film due to the thermal treatment is explained by the following model. *Figure 6* shows schematic drawings of cross-sectional views of the surface structure of the nanocomposite film before (a) and after (b) thermal treatment. During the thermal treatment, the acrylic polymer decomposed and only the silica network[26] was left with pores at the positions where the acrylic polymer existed. The apparent size of the silica particles after the thermal treatment (*Figure 6b*) is about twice as large as that of the silica or acrylic polymer domain before thermal treatment (*Figure 6a*). The pore size in *Figure 6b* is depicted to be 2–15 nm in diameter as estimated by our d.s.c. data. This heat-treated surface becomes rough compared with that before the thermal treatment. Generally, the AFM tip cannot penetrate into the pores completely due to its finite size and hence we observe the increase in the roughness and the appearance of the silica particles after thermal treatment.

CONCLUSIONS

We applied SFM techniques to investigate the microstructure and microphase separation of acrylic polymer–silica nanocomposite surfaces, which cannot be observed by SEM. We found that the acrylic polymer and the silica on the nanocomposite surface exhibited inhomogeneity with domain sizes from several to 30 nm, which were in agreement with the bulk result by d.s.c. The nanocomposite surfaces heated at 600°C, which is above the thermal decomposition temperature of acrylic polymer, showed an increase in the surface roughness. This topography change results from uncovered silica particles 20–60 nm in diameter which were partially buried under the acrylic polymer. We demonstrated that SFM will become a new surface characterization tool which is capable of not only observing microstructures, but also characterizing different materials on surfaces on the nanometre scale in air.

ACKNOWLEDGEMENTS

This work was supported by the New Energy and Industrial Technology Development Organization (NEDO).

REFERENCES

1 Saegusa, T. and Chujo, Y. *Makromol. Chem., Macromol. Symp.* 1992, **64**, 1
2 Ravaine, D., Seminel, A., Charbouillot, Y. and Vincens, M. *J. Non-Cryst. Solids* 1986, **82**, 210
3 Nakanishi, K. and Soga, N. *J. Am. Ceram. Soc.* 1991, **74**, 2518
4 Saegusa, T. and Chujo, Y. *J. Macromol. Sci., Chem.* 1990, **A27**, 1603
5 Binnig, G., Quate, C. F. and Gerber, C. *Phys. Rev. Lett.* 1986, **56**, 930
6 Mate, C. M., McClelland, G. M., Erlandsson, R. and Chiang, S. *Phys. Rev. Lett.* 1987, **59**, 1942
7 Maivald, P., Butt, H. J., Gould, S. A. C., Prater, C. B., Drake, B., Gurley, J. A., Elings, V. B. and Hansma, P. K. *Nanotechnology* 1991, **2**, 103
8 Binnig, G., Rohrer, H., Gerber, C. and Weibel, E. *Phys. Rev. Lett.* 1983, **50**, 120
9 Motomatsu, M., Nie, H.-Y., Mizutani, W. and Tokumoto, H. *Jpn J. Appl. Phys.* 1994, **33**, 3775
10 Motomatsu, M., Mizutani, W., Nie, H.-Y. and Tokumoto, H. in 'Forces in Scanning Probe Methods' (Eds H.-J. Güntherodt, D. Anselmetti and E. Meyer), Kluwer Academic, Dordrecht, The Netherlands, 1995, p. 331
11 Reifer, D., Windeit, R., Kumpf, R. J., Karbach, A. and Fuchs, H. *Thin Solid Films* 1995, **264**, 148
12 Takahashi, T. (in preparation)
13 Meyer, E., Overney, R., Lüthi, R., Brodbeck, D., Howald, L., Frommer, J., Güntherodt, H.-J., Wolter, O., Fujihira, M., Takano, H. and Gotoh, Y. *Thin Solid Films* 1992, **220**, 132
14 Meyer, G. and Amer, N. *Appl. Phys. Lett.* 1990, **57**, 2089
15 Patton, T. C. 'Paint Flow and Pigment Dispersion', Wiley Interscience, New York, 1964
16 Cassie, A. B. D. *Disc. Faraday Soc.* 1948, **3**, 11
17 Sneddon, J. N. *Int. J. Eng. Sci.* 1965, **3**, 47
18 Heuberger, M., Dietler, G. and Schlapbach, L. *Nanotechnology* 1995, **6**, 12
19 Nielsen, L. E. 'Mechanical Properties of Polymers', Reinhold, New York, 1967, p. 7
20 Burnham, N. A. and Colton, R. J. *J. Vac. Sci. Technol.* 1991, **A9**, 2548
21 Shultz, A. R. and Young, A. L. *Macromolecules* 1980, **13**, 663
22 Utracki, L. A. (transl. by Nishi, T.) 'Polymer Alloys and Blends', Tokyo Kagaku Dojin, Tokyo, 1991, p. 4
23 Kaplan, D. S. *J. Appl. Polym. Sci.* 1970, **20**, 2615
24 Bair, H. E. and Warren, P. C. *J. Macromol. Sci. Phys.* 1981, **B20**, 381
25 Saegusa, T. *Pure Appl. Chem.* 1995, **67**, 1965
26 Chujo, Y., Ihara, E., Kure, S., Suzuki, K. and Saegusa, T. *Makromol. Chem., Macromol. Symp.* 1991, **42/43**, 303